

Article

Numerical Study on the Effects of Partial Oxidation Fuel Reforming (POFR) on the Performance of a Natural Gas Engine

Mingda Wang¹, Rui Zhou², Min Guan¹, Jian Zheng² and Fei Yi^{1,*}

¹ Chinese Research Academy of Environmental Sciences, Beijing 100012, China; wangmingda@vecc.org.cn (M.W.); guanmin@vecc.org.cn (M.G.)

² Shanghai Motor Vehicle Inspection Certification & Tech Innovation Center Co., Ltd., Shanghai 201805, China; ruiuz02@smvic.com.cn (R.Z.); jianz@smvic.com.cn (J.Z.)

* Correspondence: yifei@vecc.org.cn

Abstract: Due to the issues of low flame speed and high CH₄ emissions for a natural gas engine, investigations into the partial oxidation fuel reforming (POFR) method used in natural gas engines to blend H₂ have become increasingly valuable. In this paper, the combustion process, engine performance, and emissions of a natural gas engine with fuel-reforming gases blended together have been numerically studied. The results show that a higher fuel-reforming ratio can effectively improve the engine combustion performance, especially at lean-burn conditions. Combustion with reformed gases can increase the thermal efficiency by almost 2% at the full-load condition, whereas fuel reforming significantly affects the natural gas engine's power performance. Furthermore, CH₄ and NO_x emissions decrease significantly with increasing fuel-reforming ratio. In conclusion, fuel reforming for a natural gas engine has a promising future in reducing greenhouse gas emissions and improving economic performance.

Keywords: natural gas engine; numerical simulation; partial oxidation fuel reforming (POFR); combustion and emissions; performance analysis



Citation: Wang, M.; Zhou, R.; Guan, M.; Zheng, J.; Yi, F. Numerical Study on the Effects of Partial Oxidation Fuel Reforming (POFR) on the Performance of a Natural Gas Engine. *Energies* **2023**, *16*, 7909. <https://doi.org/10.3390/en16237909>

Received: 18 October 2023

Revised: 24 November 2023

Accepted: 29 November 2023

Published: 4 December 2023



Copyright: © 2023 by the authors. Licensee MDPI, Basel, Switzerland. This article is an open access article distributed under the terms and conditions of the Creative Commons Attribution (CC BY) license (<https://creativecommons.org/licenses/by/4.0/>).

1. Introduction

With energy and environmental issues receiving more and more attention, research on alternative energy sources has become a hot topic in recent years [1]. Due to its abundant reserves; low price [2]; easy transportation; and lower CO₂, CO, and non-methane HC [3] emissions than gasoline; higher octane number, which allows for a higher compression ratio and which may enhance engine thermal efficiency [4], natural gas, whose main component is methane, has gained much attention and great potential among the many alternative energy sources for vehicles. As the number of natural gas vehicles has grown rapidly worldwide, many researchers have investigated the relevant properties of natural gas engines from different application scenarios as well as unused research methods.

However, natural gas has a slower flame spread than gasoline and diesel, which could cause problems with long burn duration and incomplete combustion [5]. It could also easily reduce engine power output and more incompletely burn natural gas fuel in the exhaust, reducing the engine's economic performance. Hence, hydrogen-blended combustion has been proposed to improve the performance of natural gas engines and recently became a hot research topic. For natural gas engines, adding hydrogen could significantly reduce CO and HC emissions, as well as enhance thermal efficiency at specific operating conditions [6,7]. Moreover, under lean combustion conditions, adding hydrogen can effectively increase the lean combustion limitation of the engine, thus reducing NO_x emissions and achieving higher thermal efficiency owing to a higher excess air ratio [8,9].

While the advantages of adding hydrogen are attractive for natural gas engines, its on-board storage remains challenging. Therefore, a novel method for producing hydrogen on-board was proposed by Southwest Research Institute, called Dedicated-Exhaust Gas

Recirculation (D-EGR) [10,11]. It can achieve fuel reforming by modifying the engine exhaust system to control the rich combustion in a specific cylinder. Then, the reforming natural gas can be recycled from the reformed cylinder to the intake system. Subsequently, Robert Mitchell et al. [12] applied this D-EGR technology to a natural gas engine. It was found that thermal efficiency can be increased by up to 11% under certain operating conditions, significantly improving engine performance. Moreover, several other popular hydrogen production technologies, such as steam methane reforming (SMR) and water–gas shift (WGS), have also been proven to reduce NO_x emissions and to improve thermal efficiency for the engine on-board fuel reforming [13–15]. However, it is quite difficult to achieve high hydrogen production rates with these technologies [9]. Furthermore, using these technologies would be more likely to cause the deterioration of HC emissions and durability for natural gas engines [12,15–17].

Therefore, the partial oxidation fuel reforming (POFR) method has been proposed and gradually developed to be a promising technology for hydrogen production in internal combustion engines [18]. By utilizing exhaust heat, on-board fuel reformers for POFR can use exhaust heat to drive their endothermic reactions. Thus, some of the waste heat can be recovered, and no additional energy is required to promote the reaction. It should also be noted that the main products of the POFR reaction are CO and H_2 , without generating large amounts of water and CO_2 [19]. Meanwhile, POFR does not require a dedicated cylinder for fuel reforming, effectively avoiding excessive engine cycling variations under specific loads. By investigating the performance of natural gas engines blended with fuel reforming mixtures, it was found that the performance and emissions of natural gas engines blended with POFR mixtures could be significantly improved under low-load conditions [20]. However, the existing research only concerned low-load conditions, and almost no publications have been released to provide systematical analyses of the effects of POFR on engine combustion performance.

On this basis, the effects of POFR on the performance of a natural gas engine were explored in this study using a numerical method. To investigate the combustion process, engine performance, and emissions of the natural gas engine with blended fuel reforming gas, a reforming natural gas–natural gas fuel–natural gas engine model was established and developed. Under different loads, the findings of this study initially revealed the characteristics of combustion and emissions from natural gas engines with blended reforming natural gas products in different proportions.

2. Numerical Method

2.1. Engine and Simulation Model

In this study, the simulation model was built based on the natural gas engine test bench and the model was calibrated based on the experimental data. The engine specifications are shown in Table 1. The schematic diagram of the partial oxidation reforming system for a natural gas engine is shown in Figure 1. Figure 1 is mainly used to illustrate the structure of the fuel reforming system, and an air filter was added into the intake system, which is important for measuring the real air flow rate and maintaining the stability of the air intake system [21].

As shown in Figure 2, a one-dimensional engine simulation model was constructed for a natural gas engine with the software GT-Power (GT-SUITE v2016). In order to provide a good prediction of in-cylinder combustion, the model involves the engine's cylinder geometry, ignition timing, fuel characteristics, etc. A turbulent flame combustion model was used to predict in-cylinder burn rate, emissions, and flame–wall interactions and calculated based on detailed cylinder geometry. The in-cylinder heat transfer was calculated with the classical Woschni correlation. And, the flow model was used to calculate the swirl, tumble, and turbulence parameters according to the piston and cylinder geometry.

Table 1. Specifications of the test engine.

Engine Parameters	Specifications
Number of cylinders	6
Bore × Stroke (mm)	128 × 153
Displacement (L)	12
Compression ratio	12:1
Rated power (kW)	310
Rated speed (rpm)	1900
Maximum torque(N m)	1750
Maximum torque related speed (rpm)	1400
Combustion mode	Lean burn

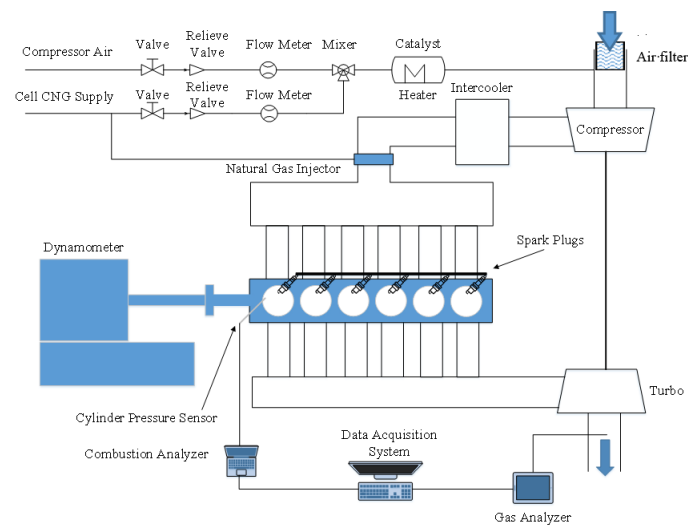


Figure 1. Schematic diagram of the experimental system.

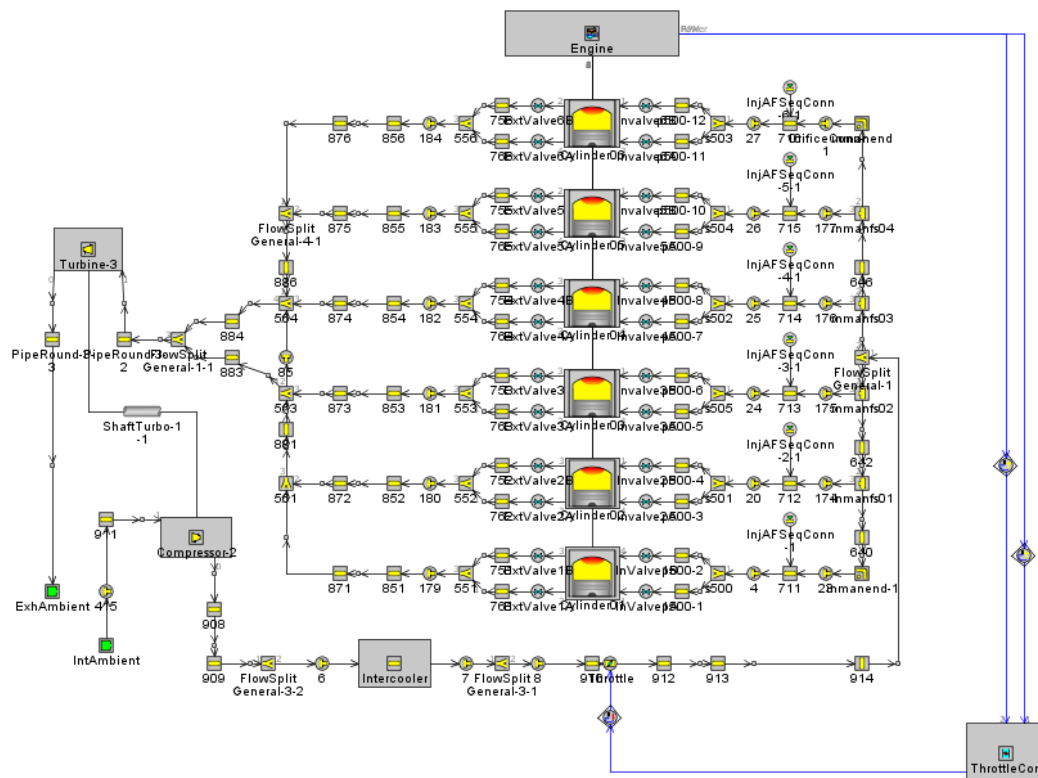


Figure 2. The simulation model for the natural gas engine.

In this model, an Explicit Euler integration scheme that is second-order accurate is used in the solver. The solver was considered to converge when the error in the parameters of temperature, pressure, and flow within the engine model was less than 2% between two consecutive steady state cycles. The time step of this simulation model is a single cycle, and the engine parameters at the end of the previous cycle will be used in the initial state of the next cycle.

Since the fuel used in the model is a mixture of natural gas and its reforming products, it is necessary to provide relevant parameters for the fuel in the engine simulation model. The basic combustion parameters of the fuel mixture were calculated using the software Chemkin-pro (Chemkin 4.5). The “Foundational Fuel Chemistry Model (FFCM-1)” was chosen to calculate the combustion parameters of the fuel mixture. For POFR, the H₂, CO, CH₄, and a small number of CO₂ components of the reforming natural gas are injected directly into the inlet pipe as part of the fuel in the injector of the engine model together with the natural gas. The N₂ component in the reforming gas is influenced by adjusting the N/O ratio in the inlet air model. The FFCM-1 reaction mechanism was used to simulate the combustion of CH₄ and the combustion of H₂, CO, CH₂O, and other components in good agreement with the actual experimental results [22]. The fuel mixture’s maximum laminar flame propagation velocity and the corresponding reaction equivalent ratio at this velocity can be obtained. In addition, as shown in Equations (1) and (2), parameters such as flame decay velocity, temperature coefficient, and pressure coefficient of the mixed fuel were calculated using empirical methods [23,24].

$$S_L = S_{L,ref} \left(\frac{T_U}{T_{U0}} \right)^\alpha \left(\frac{P_U}{P_{U0}} \right)^\beta (1 - 2.1Y_{dil}) \quad (1)$$

$$S_{L,ref} = B_M + B_2(\phi - \phi_M)^2 \quad (2)$$

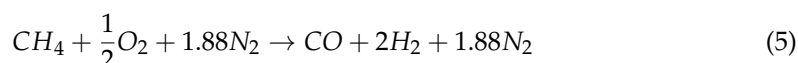
where S_L denotes the laminar flame burning velocity of the mixed fuel; Y_{dil} denotes the mass fraction of dilution gas in the air–fuel mixture; $S_{L,ref}$ denotes the laminar flame propagation velocity of the mixed fuel in the reference state; B_M denotes the maximum laminar flame burning speed of the fuel mixture; B_2 denotes the laminar flame decay velocity of the fuel mixture; ϕ denotes the actual equivalent ratio for the natural gas engine at different operating conditions; and ϕ_M denotes the equivalent ratio for the conditions corresponding to the maximum laminar flame burning speed of the fuel mixture.

To obtain an explicit expression about laminar burning velocities dependent on pressure and temperature, the measured laminar burning velocities have been fit to a simple power law relation at the datum temperature T_{U0} (300 K) and the datum pressure P_{U0} (0.1 Mpa). T_U and P_U are the in-cylinder temperature and pressure, respectively. Moreover, both the temperature coefficient α and the pressure coefficient β are functions of the chemical equivalence ratio and are calculated using Equations (3) and (4):

$$\alpha = 5.75\phi^2 - 12.15\phi + 7.98 \quad (3)$$

$$\beta = -0.925\phi^2 + 2\phi - 1.473 \quad (4)$$

Moreover, Equation (5) demonstrates that POFR is achieved by reforming natural gas with air, resulting in fast self-heating that can be sustained without a continuous heat supply. An Rh-based catalyst is used to carry out POFR at an inlet gas temperature of 300 °C, an inlet pressure of 1 bar, and a reaction velocity of 25,000 h⁻¹. Studies indicate that hydrogen production rates can reach up to 60% when the fuel-reforming ratio ranges between 3% and 12% [18].



Regarding the blended fuel of the natural gas engine, the mixture components can be calculated after blending different proportions of fuel-reforming gas based on the POFR products. In this study, the fuel blends for the natural gas engine were mixed with 0%, 3%, 6%, 9%, and 12% of fuel reforming gas, and the key information is listed in Table 2. Furthermore, as shown in Equation (6), a parameter, fuel-reforming ratio (F), is introduced to help clearly illustrate the ratio of fuel which is involved in POFR.

$$F = \frac{FC_R}{FC_C} \times 100\% \quad (6)$$

where FC_R denotes the fuel mass flow rate participating in the reforming reaction, and its unit is kg/h; FC_C denotes the fuel consumption under the same load conditions for the natural gas engine, and its unit is kg/h.

Table 2. Blended fuel components with different proportions of reforming natural gas.

Fuel reforming ratio (%)	Blended Fuel Components				
	0	3	6	9	12
CNG (%)	100	95.3	89.6	85.7	79.3
H ₂ (%)	0	3.0	6.6	9.3	13.4
CO (%)	0	1.3	3.1	4.1	6.1
CO ₂ (%)	0	0.4	0.7	0.9	1.2

Figure 3 shows the calculation results of natural gas fuel laminar flame speed, where F0 is the fuel-reforming ratio of 0 (pure natural gas) and F12 is the fuel-reforming ratio of 12%. It can be seen that as the fuel-reforming ratio increases from 0% to 12%, the maximum laminar flame burning speed increases with the increasing H₂ content in the fuel, with the maximum laminar flame velocity corresponding to equivalence ratios ranging from 1.05 to 1.10 for different types of fuel blends. The maximum laminar flame velocities for F0 and F12 are each 0.37 m/s and 0.41 m/s, while both have the maximum laminar flame velocity at an equivalence ratio of around 1.08.

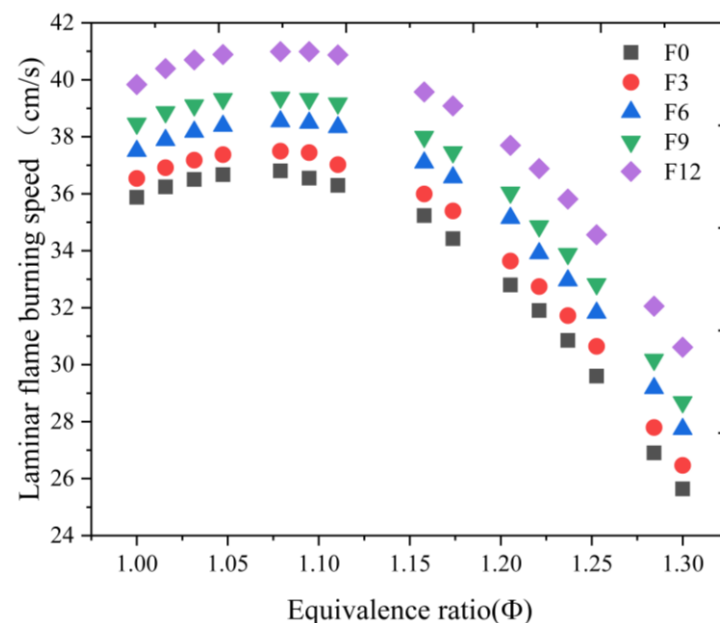


Figure 3. Natural gas fuel laminar flame speed calculation results.

Table 3 gives the low calorific values of the mixed fuel in the natural gas engine simulation model.

Table 3. Low calorific value corresponding to blended fuels with different proportions of reforming natural gases.

Fuel reforming ratio (%)	0	3	6	9	12
Low calorific value (MJ/kg)	48.6	47.5	46.2	45.5	44.0

2.2. Natural Gas Engine Simulation Model Validation

The natural gas engine has been tested on the engine test bench under low- and medium-load conditions with different fuel-reforming ratios. Therefore, these test data can be used to validate the POFR natural gas engine simulation model.

During the bench test, the emission of gaseous pollutants was measured with an AVL 493D GAS PEMS device, and the fuel flow rate and air flow rate were measured separately with TOCEIL CMF050 and FMT700-P. The engine combustion parameters (in-cylinder pressure, heat release rate, etc.) were measured and calculated with AVL Indicom. Table 4 shows the accuracy of all the measuring equipment.

Table 4. The accuracy of measuring equipment.

Measurements	Measurement Range	Accuracy
Power	0~450 kW	±1 rpm
Torque	0~2500 Nm	±1 Nm
Fuel flow rate	0~150 kg/h	±0.1 kg/h
Air flow rate	0~3000 kg/h	±0.8% measured value
NO _x	0~5000 ppm	±5 ppm
THC	0~30,000 ppm	±5 ppm
CO	0~5000 ppm	±2 ppm
Temperature	0~1000 °C	±1 °C
Pressure	80~120 kPa	±1 kPa

The reformed fuel and air flow rates were controlled with flow meters and pressure-regulating valves, respectively, and the reformed gases were mixed with the intake air before the inlet of the supercharger. And, after the engine had run steadily for 3 minutes, the relevant equipment recorded the engine performance and emission parameters under this operating condition. The flow rates of fuel and air involved in the reforming reaction were calculated on the basis of the fuel-reforming ratio.

According to the basic combustion parameters calculated with Chemkin-pro, the combustion model and fuel model have been set up and calibrated using experimental data from the natural gas engine test bench of Figure 1. The intake and exhaust boundary conditions of the simulation model were consistent with the atmospheric environment in the laboratory when the engine was under partial-load conditions, and the intake and exhaust pressures were set according to the actual measurements on the test bench. Under full-load conditions, the engine simulation model's pressure and temperature after the outlet of the supercharger were set to be consistent with the bench test values (under pure natural gas fuel conditions), and the exhaust boundary conditions were consistent with the laboratory atmosphere.

The cylinder pressure was compared and validated at partial-load conditions at 1500 rpm with a 12% reforming natural gas. As shown in Figure 4, the experimental and the simulated data of cylinder pressure show consistency in terms of maximum peak pressure and combustion phase, indicating that the model could better reflect the actual combustion situation in the engine.

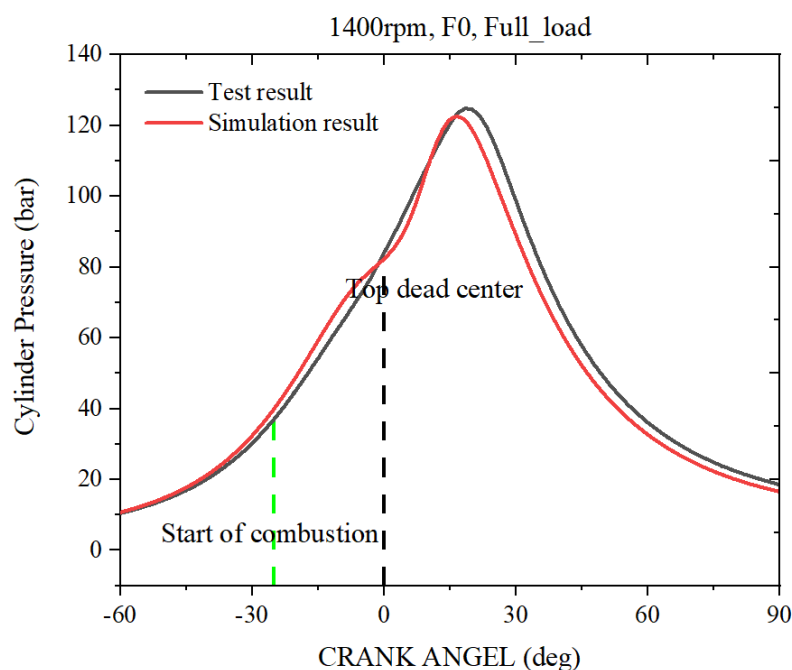


Figure 4. Comparison of cylinder pressure curves for partial load blending of 12% reforming gas at 1400 rpm.

Moreover, Figure 5 compares the engine's maximum power, intake air flow rate, and brake-specific fuel consumption (BSFC) under different operating conditions. The relevant in-cylinder combustion equivalent ratios and ignition advance angles at full-load conditions are shown in Table 5. The maximum power result shows a strong correlation between the experimentally obtained data and the model-calculated values, with negligible deviation observed between 1300 rpm and 1500 rpm. As the engine speed increases, the discrepancy between the measured and simulated values was found to be 3.4% at 1700rpm. Moreover, the disparity in BSFC tends to decrease with increasing speeds, with the highest difference of 4.1% observed at 1300 rpm. For the partial-load conditions, the measured and simulated data showed comparable values for BSFC and intake air mass flow rate, with the exception of the 10% load at 1500rpm. In this case, the BSFC error was noted as 9.2%. The error between the experimental and simulated results for most of the compared conditions does not exceed 5%. Hence, the calculation results by the simulation model are relatively accurate and predictive.

Table 5. Equivalence ratio and spark timing of natural gas engine at full load.

Rotational Speed (r/min)	1200	1300	1400	1500	1600	1700
Equivalence ratio (ϕ)	0.655	0.652	0.65	0.65	0.65	0.645
Spark timing (deg)	-23	-24	-25	-25	-27	-29

In general, the numerical study mainly includes two sub-studies: one is to investigate the combustion characteristics of combustion and performance, and the other is for the emission characteristics. Furthermore, the two sub-studies were conducted under both partial and full loads. The engine speed of partial loads in the simulation was set to be 1500 rpm. Regarding the full load, the engine speed was set at 1200–1700 rpm with the same inlet manifold pressure.

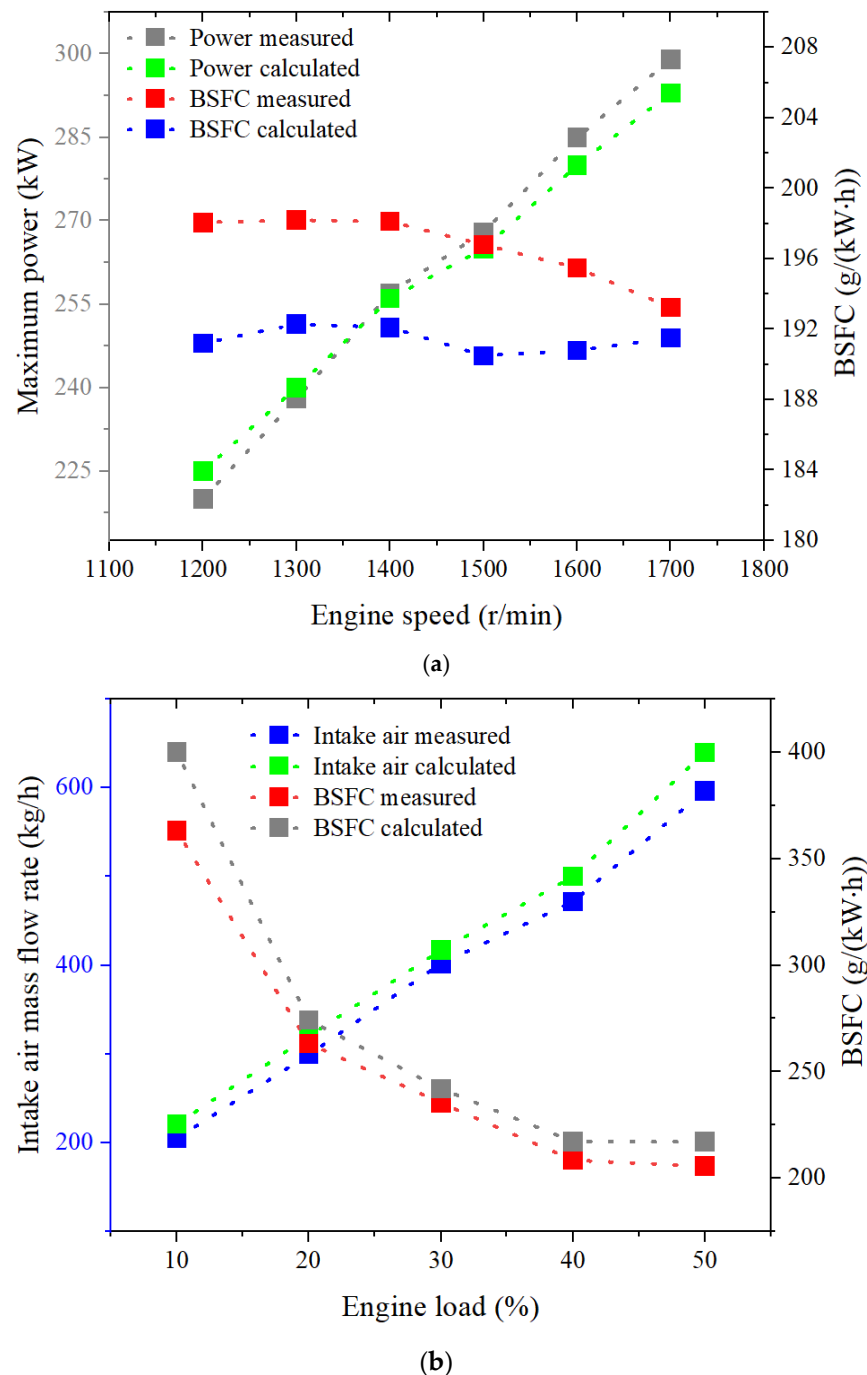


Figure 5. Comparison of intake air flow rate and specific fuel consumption under different speed and load conditions. (a) Comparison of maximum power and fuel consumption at different speed conditions. (b) Comparison of intake air flow rate and BSFC under different load conditions at 1500 rpm.

3. Results and Discussion

3.1. Characteristics of Combustion and Performance

3.1.1. Partial Load (30% Load)

Figure 6 shows the in-cylinder pressure and in-cylinder heat release rate curves at 1500 rpm and 30% load with different percentages of reforming natural gas. It can be seen that when the proportion of reforming natural gas increases, the in-cylinder pressure rise rate and heat release rate at the beginning of combustion increase significantly due to the

increase in the laminar combustion rate of the fuel blend, resulting in higher in-cylinder pressure. A higher proportion of reforming natural gas blended could bring the relative content of N_2 in the inlet gas higher and can enhance the dilution effect of N_2 , leading to slower in-cylinder combustion and lower exothermic rates.

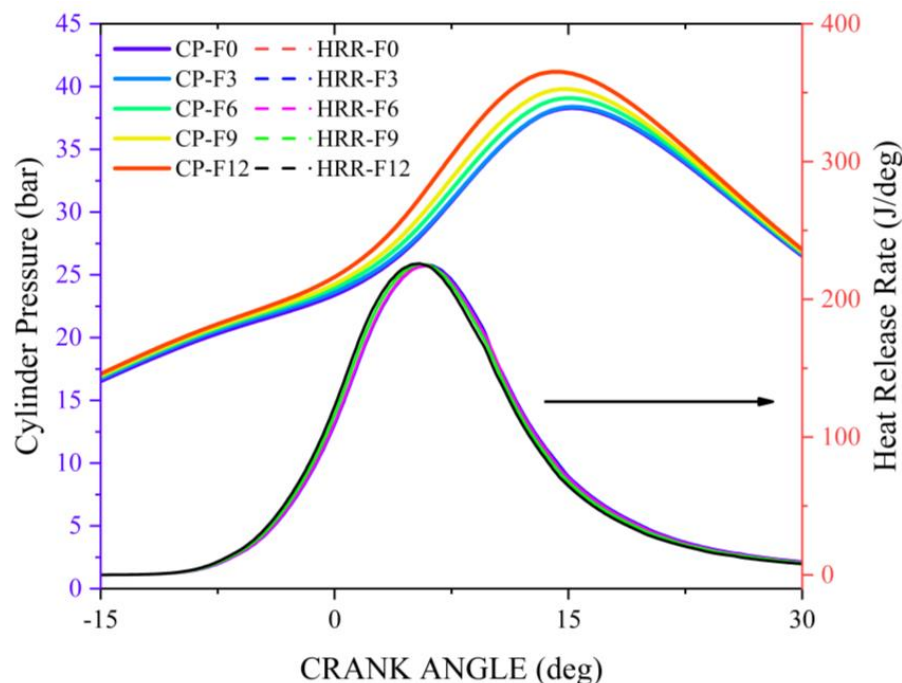
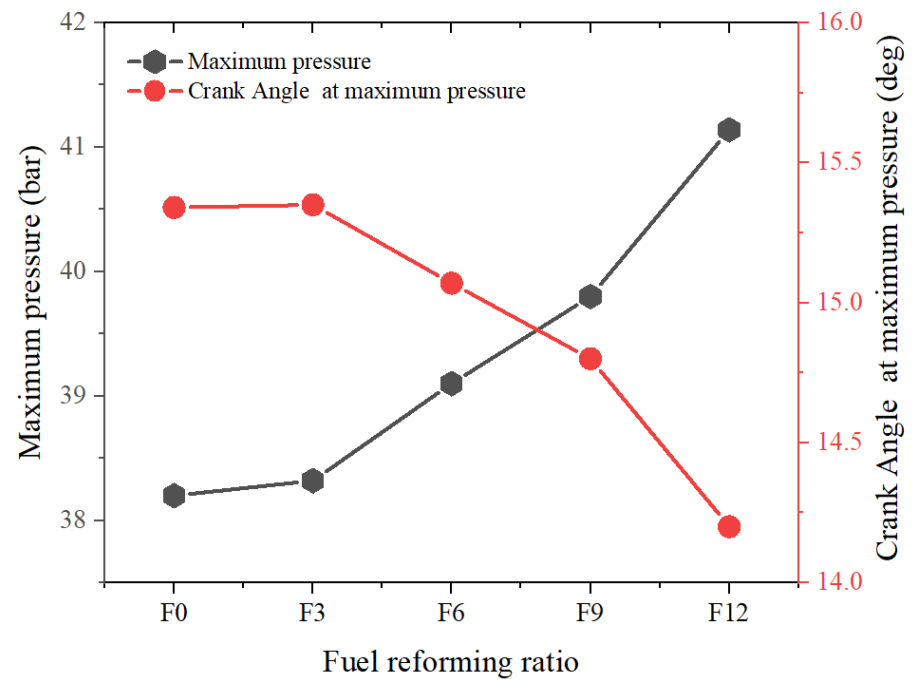


Figure 6. In-cylinder pressure and heat release rate curves with different proportions of reforming gas (The arrow in the figure indicates the heat release rate curves).

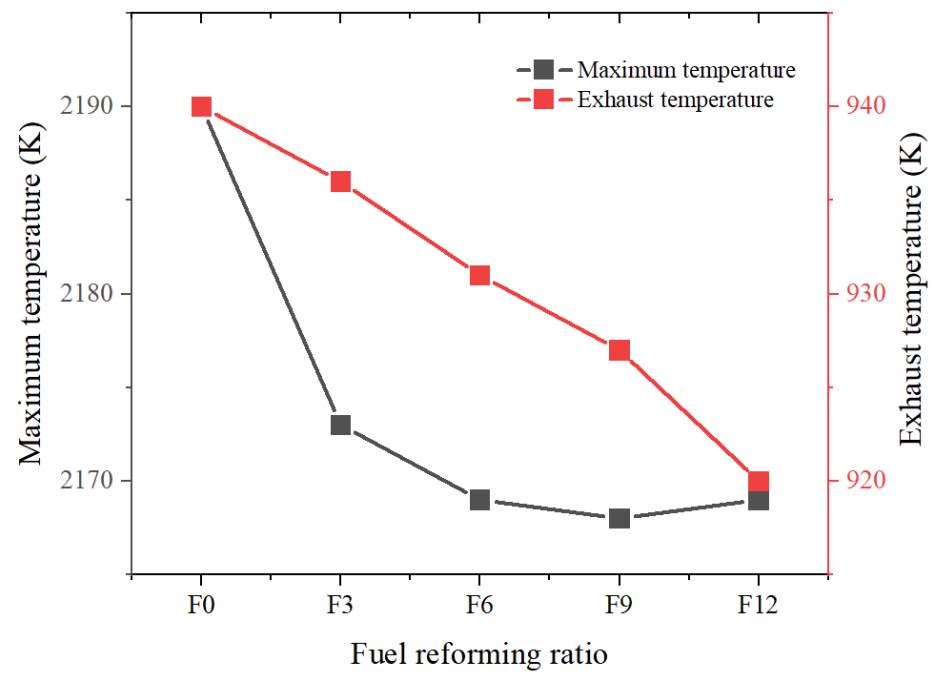
Figure 7 presents the results of key combustion performance parameters at 1500 rpm and 30% load, such as the peak in-cylinder pressure, peak in-cylinder temperature, exhaust temperature, and crankshaft angle for some combustion periods. It can be seen that the peak in-cylinder pressure increases as the reforming gas blending ratio increases, which is mainly because the accelerated combustion rate of the fuel mixture leads to an earlier crankshaft angle corresponding to the peak pressure. Moreover, the peak in-cylinder temperature decreases by increasing reforming gas blending due to the dilution effect of N_2 and CO_2 . The blending reforming gas could improve the combustion rate in the early combustion stage, which might increase fuel consumption. A gradual decrease in engine exhaust temperature can also be found with a higher reforming gas blending ratio.

In addition, both the crank angle of 2% mass fraction burnt (CA_{02}) and the crank angle of 50% mass fraction burnt (CA_{50}) advance by increasing the blending ratio of the reformer gas. For the entire combustion cycle, the effect of blending reforming natural gas on the combustion phase is not significant. The combustion duration of 0–50% and 0–90% in the cylinder change no more than 2 °CA as the reforming gas blending ratio increases.

Figure 8 shows the indicated in-cylinder thermal efficiency and BSFC with different fuel-reforming ratios. Overall, the indicated thermal efficiency increases as the reforming gas blending ratio increases. Compared to unblended reforming natural gas, an increase of nearly 1% at 12% reformed fuel is achieved. This is mainly because, according to the results in Figure 6, the reforming natural gas accelerates the in-cylinder fuel combustion, increasing the peak in-cylinder pressure. On the other hand, the presence of CO_2 and N_2 in the reforming natural gas helps reduce the maximum in-cylinder temperature and the exhaust gas temperature, decreasing the engine's heat loss.

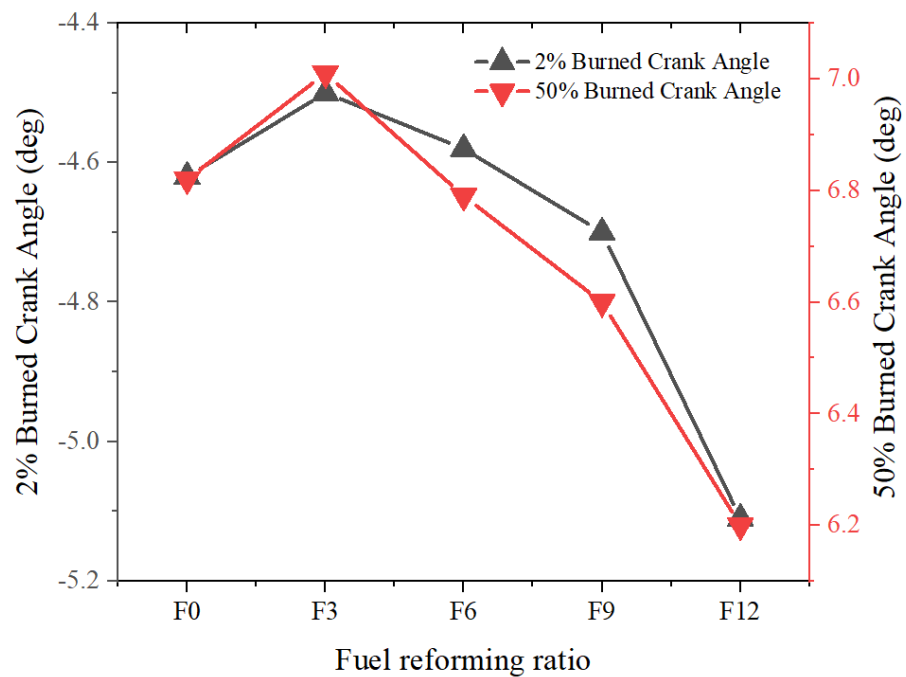


(a)

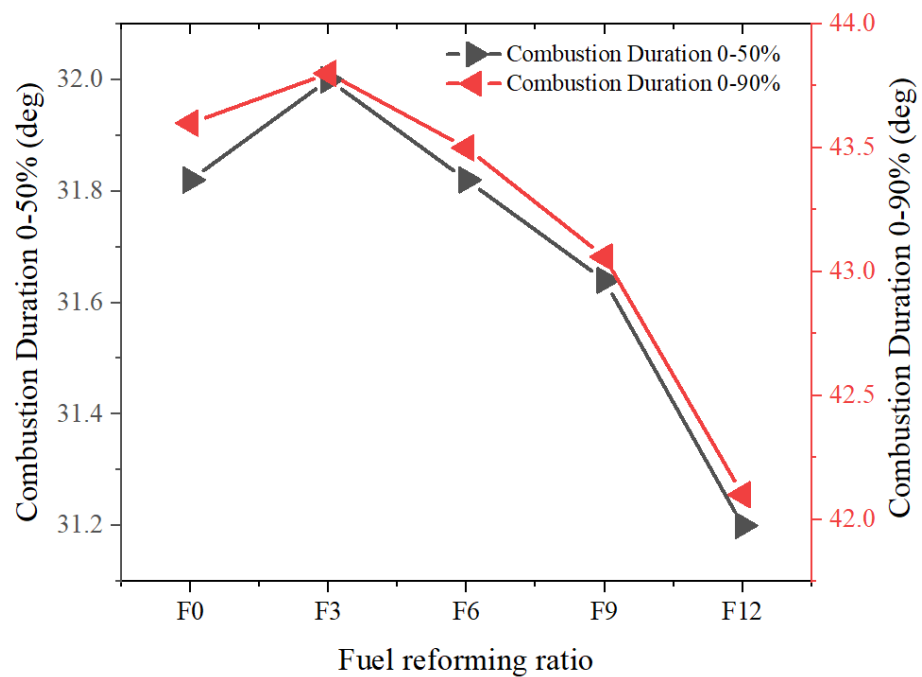


(b)

Figure 7. Cont.



(c)



(d)

Figure 7. Key parameters of combustion performance under the conditions of different reforming gas proportions. (a) Maximum in-cylinder pressure and corresponding crank angle. (b) Maximum in-cylinder temperature and exhaust temperature. (c) CA02 and CA50. (d) Combustion duration of 0–50% and combustion duration of 0–90%.

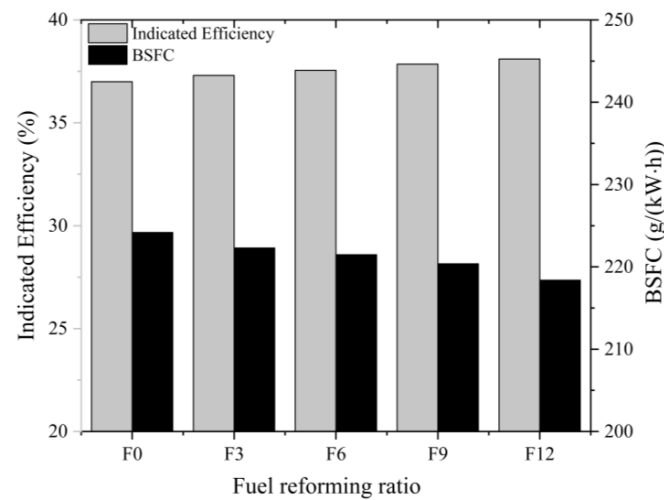


Figure 8. In-cylinder indicated thermal efficiency and specific fuel consumption corresponding to combustion with different proportions of reforming gas.

3.1.2. Full Load

Figure 9 shows the in-cylinder pressure with different fuel-reforming ratios at full load. It can be seen that the peak in-cylinder pressure increases as the fuel-reforming ratio rises from 3% to 12%. Furthermore, the crank angle of maximum peak pressure becomes closer to the TDC as the fuel-reforming ratio increases, particularly at lower engine speeds. According to Figure 9, the crankshaft angle of maximum peak pressure advanced almost 3° at 1200 rpm. In general, the engine can achieve its maximum efficiency when maximum pressure occurs at a crank angle of 10–15 degrees ATDC [25]. Furthermore, it should be noted that F3 (with a 3% fuel-reforming ratio) and F6 (with a 6% fuel-reforming ratio) exhibit slightly lower peak in-cylinder pressure than F0. Additionally, the maximum peak pressure crank angle was not found to be closer to TDC for F3 and F6, suggesting that only the fuel-reforming ratios of 9% and 12% may enhance the engine's thermal efficiency. It is noteworthy that further investigation is warranted to verify this hypothesis. This may be due to a lower fraction of H_2 in the reformed gases resulting from a low fuel-reforming ratio, which has a reduced impact on the rate of fuel combustion in the cylinder.

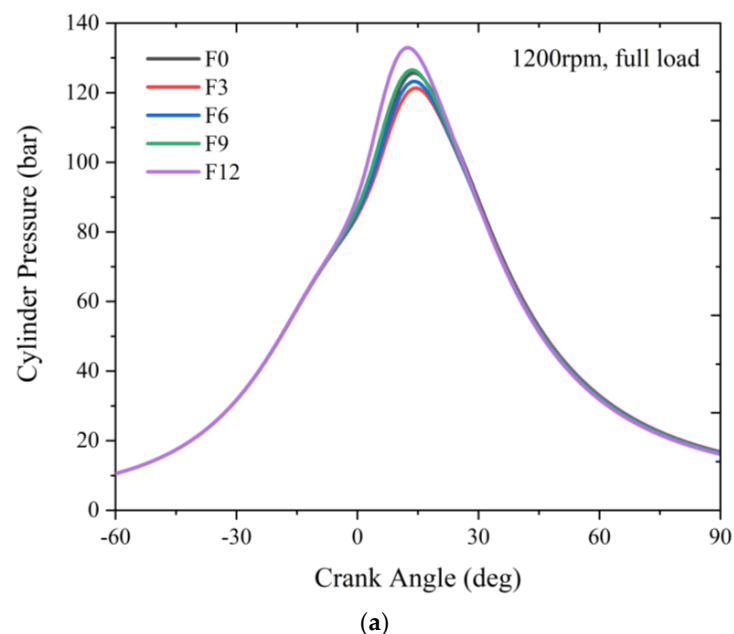


Figure 9. Cont.

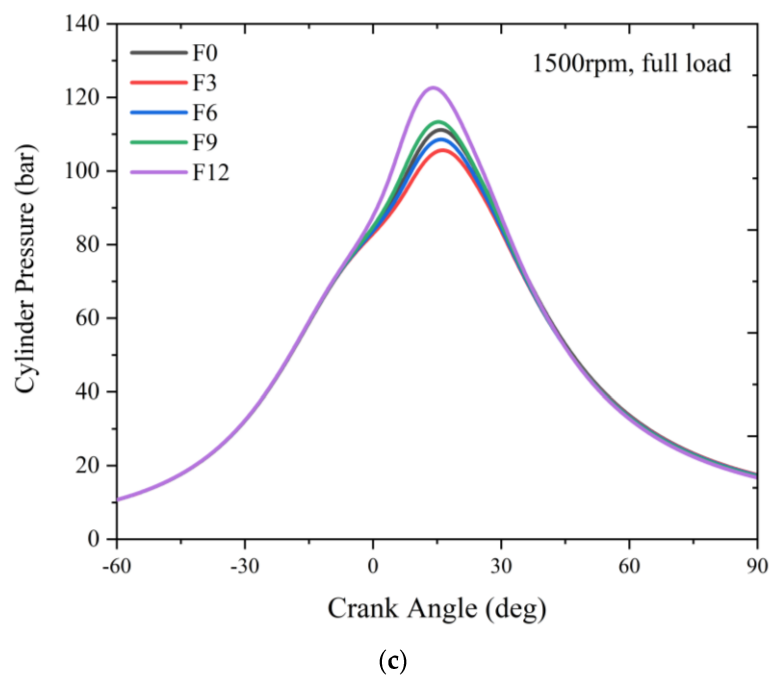
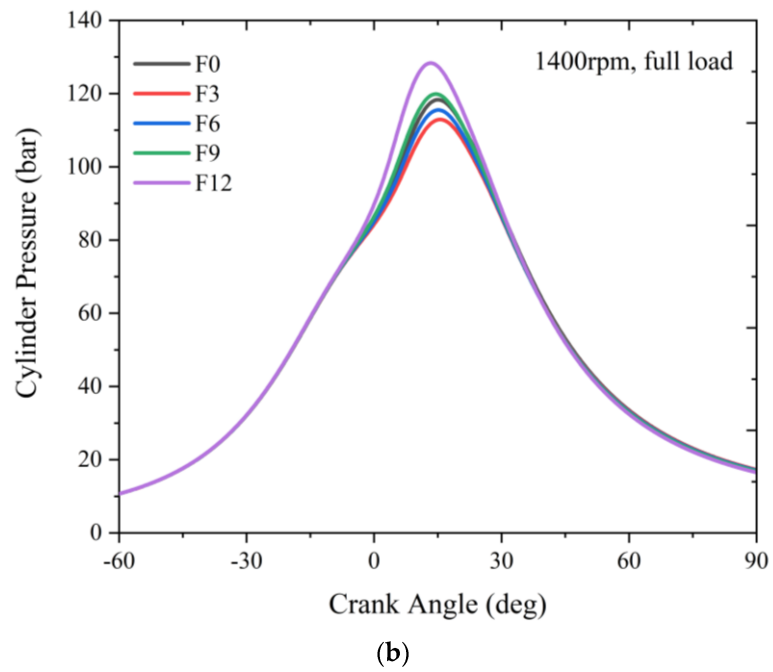


Figure 9. Cont.

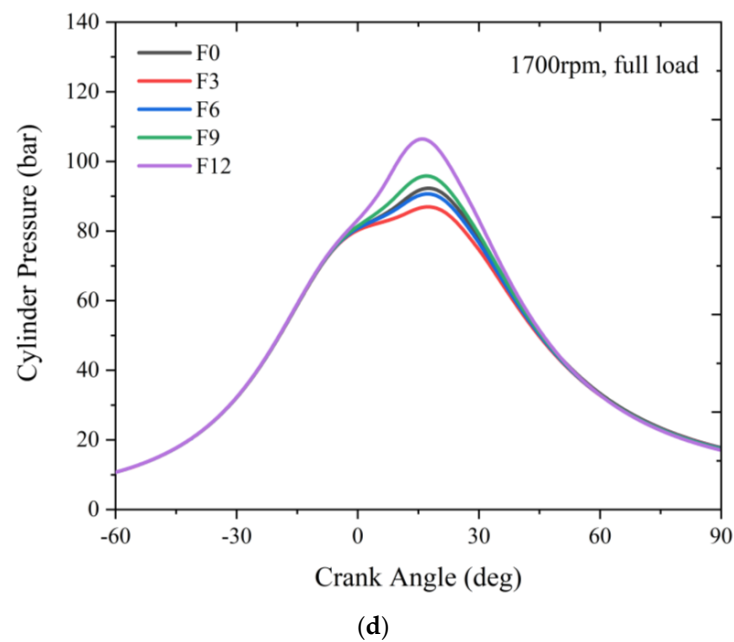


Figure 9. In-cylinder pressure corresponding to different proportions of reforming gas. (a) In-cylinder pressure at 1200 rpm. (b) In-cylinder pressure at 1400 rpm. (c) In-cylinder pressure at 1500 rpm. (d) In-cylinder pressure at 1700 rpm.

Figure 10 shows that the peak in-cylinder temperature generally increases by increasing the fuel-reforming ratio from 3% to 12%. At 1200 rpm, the peak in-cylinder temperature with blending reforming gas is lower than that of F0. As the engine speed increases, the peak in-cylinder temperature of F12 is higher than that of F0. Compared to F0, the natural gas engine in-cylinder temperature decreases more rapidly after 30 degree ATDC with reforming natural gas under all conditions. As engine speed increases, the engine's excessive air ratio also increases, and the effect of the fuel reforming on engine combustion temperature becomes more evident. Furthermore, the maximum cylinder temperature decreased when the fuel-reforming ratio was set to 3% and 6%, indicating that a low fuel-reforming ratio does not improve the combustion in the cylinder.

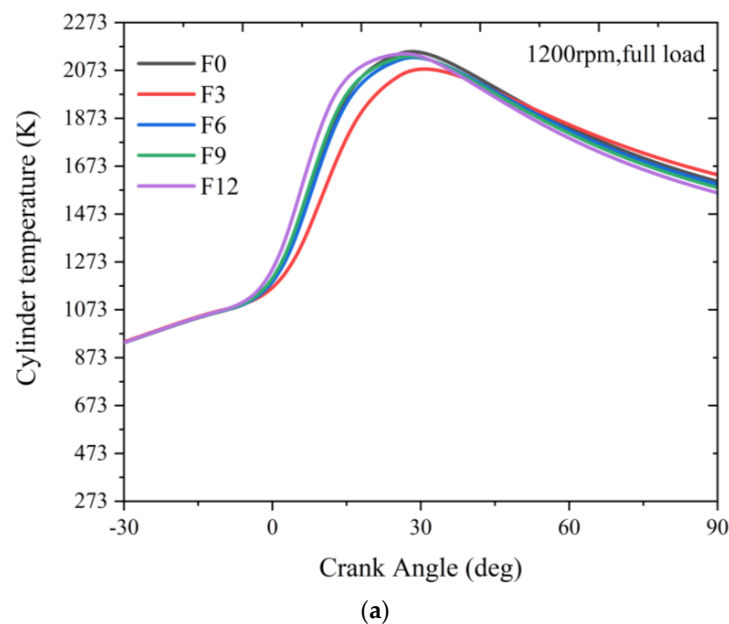
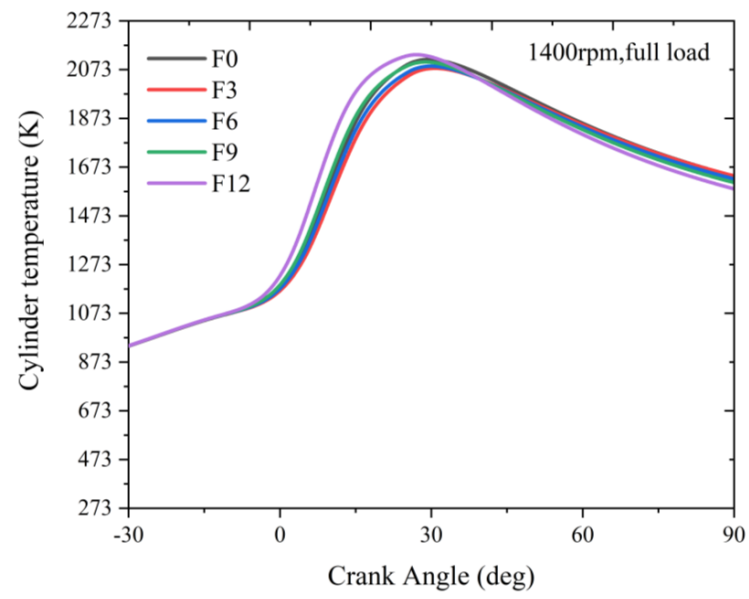
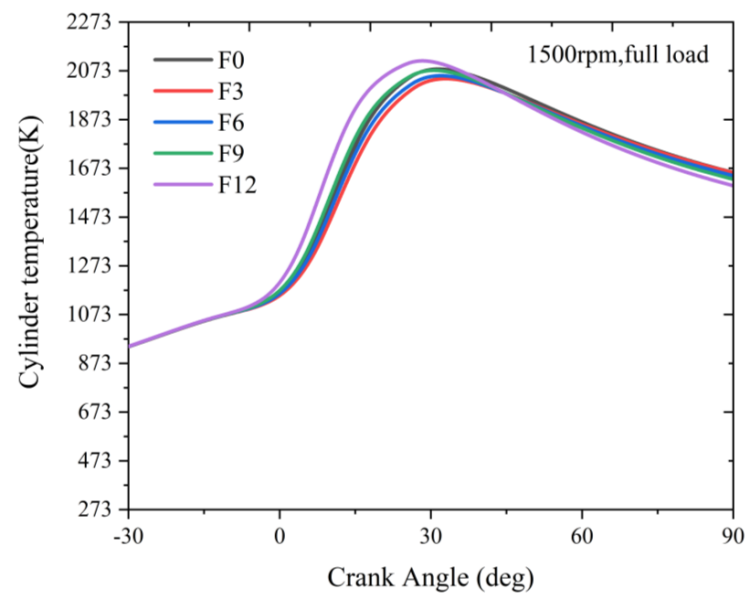


Figure 10. *Cont.*



(b)



(c)

Figure 10. Cont.

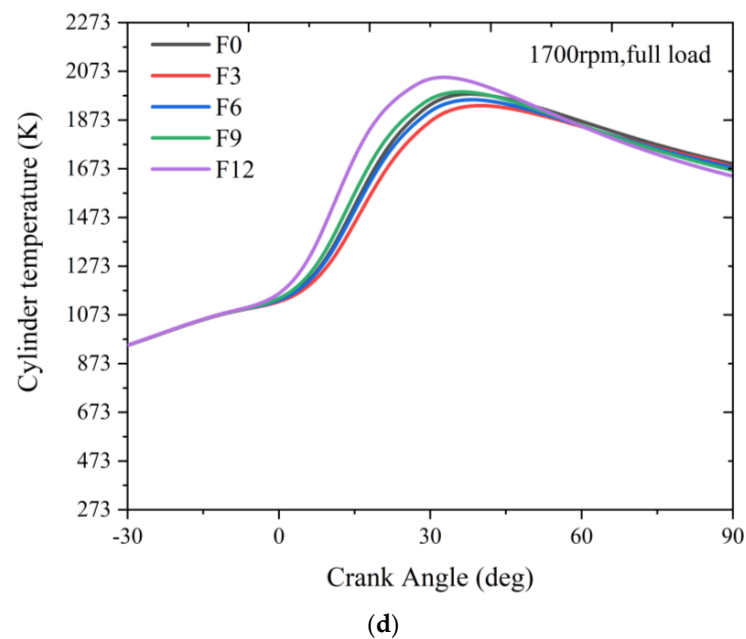


Figure 10. In-cylinder temperature corresponding to the combustion of different proportions of reforming gas. (a) In-cylinder temperature at 1200 rpm. (b) In-cylinder temperature at 1400 rpm. (c) In-cylinder temperature at 1500 rpm. (d) In-cylinder temperature at 1700 rpm.

As mentioned earlier, the H_2 component in the reforming natural gas accelerates the initial rate of in-cylinder fuel combustion. Figure 11 shows the CA50 and combustion duration 0–50% at different speeds under full-load conditions. With 12% reforming natural gas, the CA50 is advanced by about 2–3 °CA at full-load conditions for all engine speeds. Compared to F0, the combustion duration of 0–50% of F12 shortens more as the speed increases, and the gap is almost 5 °CA at 1700 rpm. This would lead to a more pronounced increase in peak in-cylinder temperature and pressure under F12 compared to F0. In addition, by raising the speed from 1500 rpm to 1600 rpm, CA50 has a tendency to slightly decrease, mainly because the in-cylinder equivalent ratio remains unchanged under both conditions, while the ignition advance angle at 1600 rpm increases, resulting in a small advanced CA50.

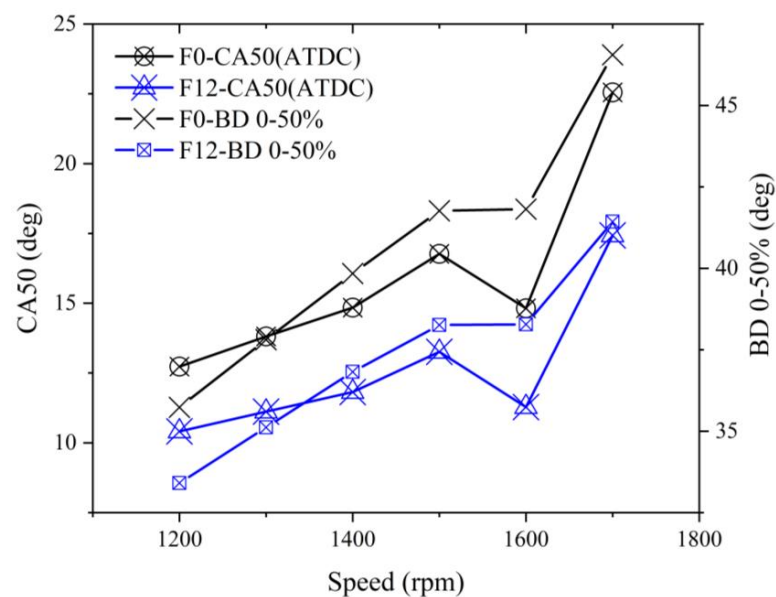


Figure 11. CA50 and combustion duration of 0–50% corresponding to different engine speeds.

As the fuel composition changes and the N/O ratio in the intake air changes with POFR, the power and economic performance of the natural gas engine will inevitably change. Figure 12 shows the power output with 12% reforming natural gas blending at full load. Compared to F0, the maximum engine power of F12 is reduced under all the speed conditions. Also, the maximum engine power difference before and after reforming natural gas blending decreases as the speed increases, with the power dropping by nearly 10 kW at 1200 rpm and by no more than 5 kW at 1700 rpm. The decrease in maximum power is mainly due to the reduced calorific value of the blended fuel. In the meantime, the intake pressure of the engine remains the same, and the intake mass flow is almost the same, resulting in lower in-cylinder combustion heat release and a reduction in engine power.

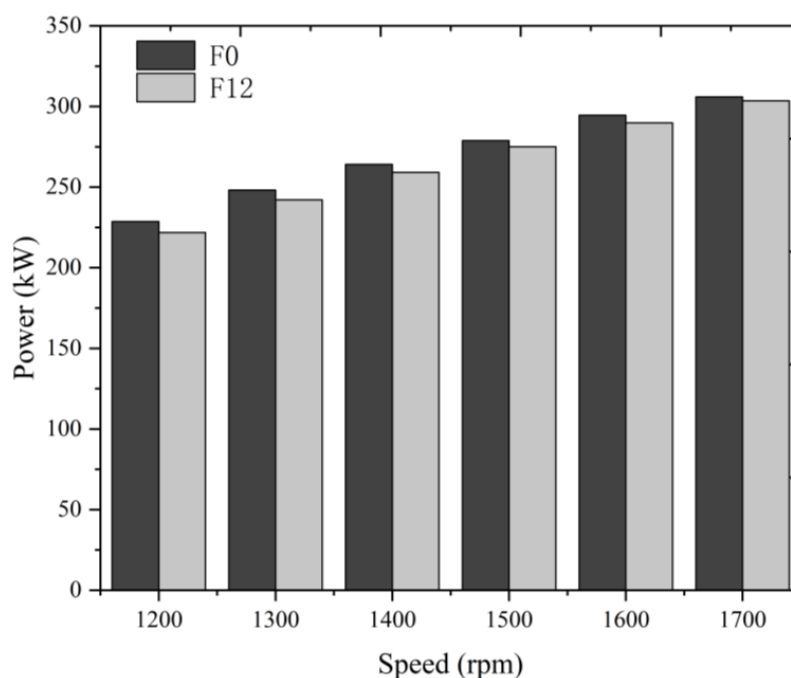


Figure 12. Maximum power corresponding to different engine speeds with 12% fuel reforming.

Figure 13 shows the cumulative in-cylinder heat release for the engine. It can be found that the trend of the cumulative in-cylinder heat release at 1200 and 1400 rpm is basically the same. As the fuel-reforming ratio increases, the accumulated in-cylinder heat release decreases throughout the combustion cycle. As the combustion continues, the cumulative heat release of the reforming natural gas blended engine starts to be lower than that of the pure natural gas fuel after 30 °CA. In addition, the combustion rate in the early stage and the in-cylinder specific heat capacity would be increased because the reforming natural gas mixture could cause a rapid drop in in-cylinder pressure and temperature, negatively affecting the engine power output.

Figure 14 shows the indicated engine thermal efficiency at 1200 rpm to 1700 rpm. As the speed increases from 1200 rpm to 1700 rpm, the indicated thermal efficiency decreases for both F0 and F12. Compared to F0, the indicated thermal efficiency of F12 increases under each speed condition. The relevant absolute improvement percentage is almost 1% and 2% for the conditions of 1200 rpm and 1700 rpm, respectively. Although the blending of the reforming natural gas reduces the maximum power (as shown in Figure 12), it is helpful in the improvement of engine thermal efficiency and economic performance.

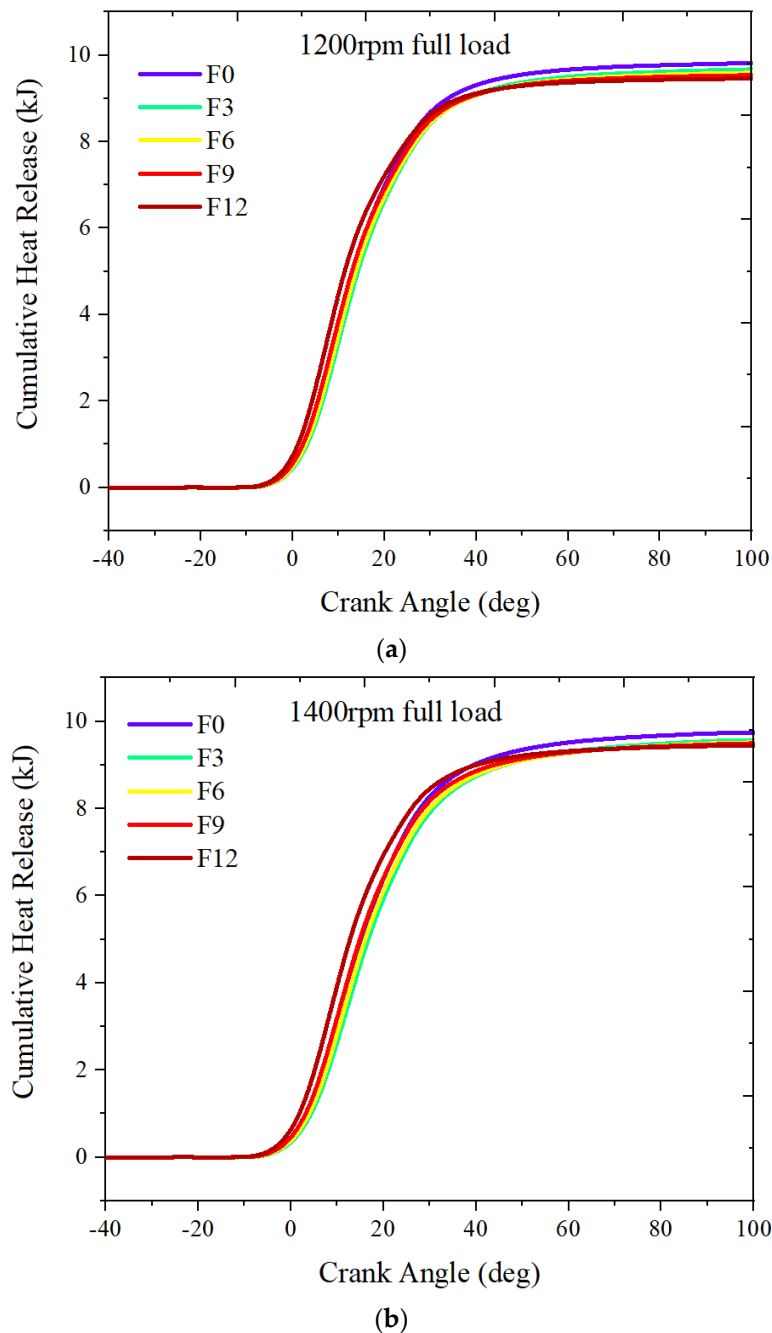


Figure 13. Cumulative heat release corresponding to different engine speeds with 12% fuel-reforming ratio. (a) Cumulative heat release at 1200 rpm. (b) Cumulative heat release at 1400 rpm.

3.2. Emission Characteristics

This section presents a simulation model to predict the gaseous emissions of the natural gas engine after blended reforming natural gas products. The NO_x model is based on an extended “Zeldovich” mechanism, the results of which are strongly influenced by the peak in-cylinder temperature. The HC model is based on a two-dimensional planar flame quenching model and a simple reaction kinetic mechanism after flame quenching, affected by the fuel flame quenching distance and the global reaction rate. The calculation of CO is based on the model in the book of *Internal Combustion Engine Fundamentals* by John B. Heywood [19]. The main reactions are shown in Equations (7) and (8).



$$K^+_{CO} = 6.76 \times 10^{10} \times e^{\frac{T}{1102}} \text{ cm}^3/\text{gmol} \quad (8)$$

where T is the maximum in-cylinder combustion temperature, and its unit is K; K^+_{CO} is the reaction rate constant.

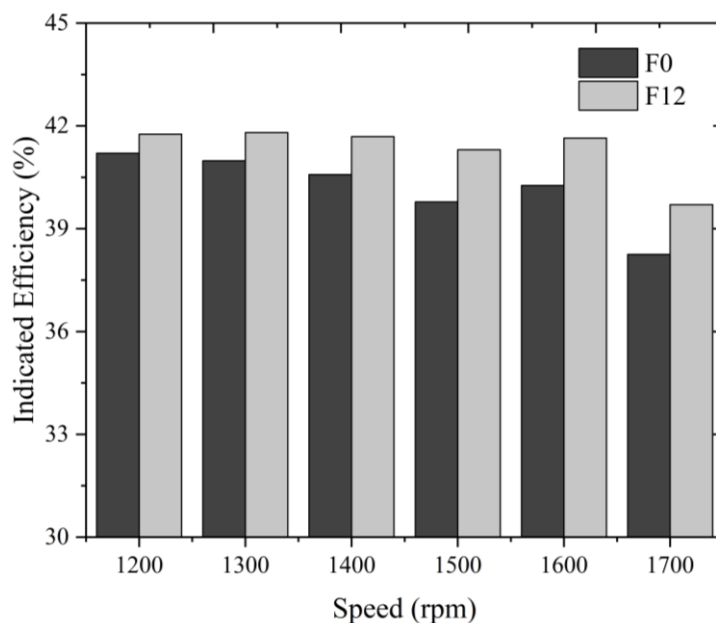


Figure 14. In-cylinder indicated efficiency corresponding to different engine speeds with 12% fuel-reforming ratio.

Figure 15 shows the gaseous emissions by blending different proportions of reforming natural gas at 1500 rpm, 30% load. Generally, NO_x and HC significantly decrease with increasing fuel-reforming ratio. This is because NO_x emissions are very sensitive to the peak in-cylinder temperature. And, the decreasing trend of HC is due to the addition of H_2 in the reforming gas, which leads to a smaller flame-quenching distance of the fuel mixture. Moreover, the increase in CO can be attributed to two main aspects. First, it is because of a gradual increase in the CO content of the fuel itself. Second, as shown in Equation (7), the decrease in peak in-cylinder temperature, combined with the increase in the fuel blend's H group content, both reduce the driving force for the positive CO oxidation reaction, leading to an apparent increase in CO.

Figure 16 below shows the NO_x for the natural gas engine at full load. It can be found that the NO_x for the natural gas engine is obviously reduced as the fuel-reforming ratio increases from 0% to 12%. The NO_x emissions at 1200 rpm are reduced by almost 20%. This is also because the in-cylinder temperature is lower than that of pure natural gas fuel throughout the combustion cycle. As mentioned in Figure 11, increasing the ignition advance angle at 1600 rpm results in a closer CA 50 to the top dead center of the engine, which would obviously increase the highest temperature in the engine cylinder, generating more NO_x .

Figure 17 below shows the CH_4 results for the natural gas engine at full load. The CH_4 from the natural gas engine blended with 12% reforming natural gas products at full load show a significant reduction. Regarding relative emissions, the CH_4 decreased by 33% at 1200 rpm and CH_4 decreased by nearly 500 ppm at 1700 rpm, representing a relative reduction of nearly 28%. This indicates that reforming gas blending has the potential to reduce CH_4 emissions for the natural gas engine greatly.

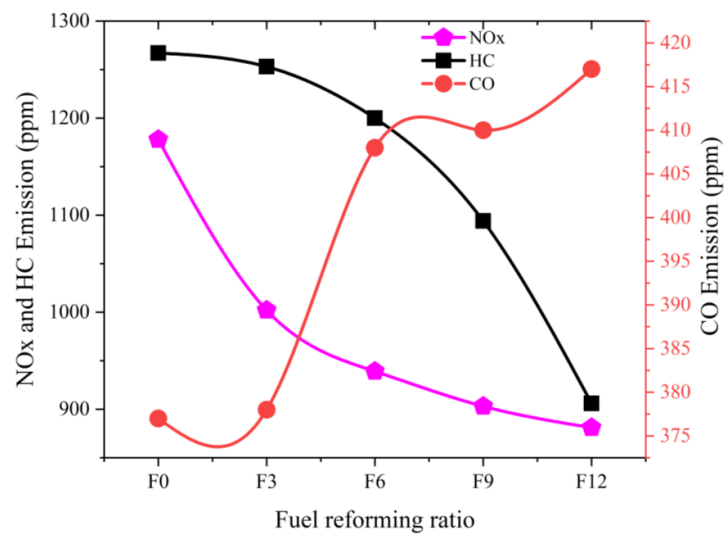


Figure 15. Gaseous pollutant emissions under different fuel-reforming ratios at 1500 rpm.

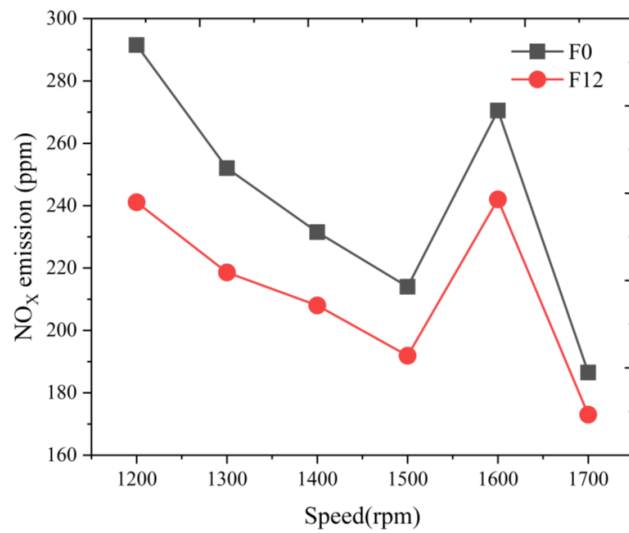


Figure 16. NO_x corresponding to different engine speeds with 12% fuel reforming.

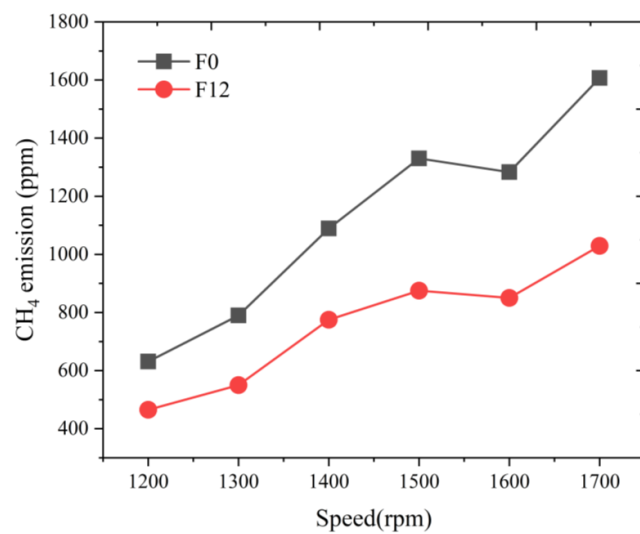


Figure 17. CH₄ corresponding to different engine speeds with 12% fuel reforming.

4. Conclusions

In this study, the combustion process, engine performance, and emissions of a natural gas engine with blended fuel-reforming ratios were systematically investigated in detail using Chemkin-pro and GT-POWER. The main findings of this study can be summarized as follows:

1. Increasing the fuel-reforming ratio results in higher peak in-cylinder temperature and pressure at full load. However, only combustion with 9% and 12% fuel-reforming gases shifted the maximum pressure crank angle closer to the TDC and increased the maximum in-cylinder pressure compared to pure natural gas. This suggests that a fuel-reforming ratio of 9% and 12% can enhance the combustion performance of natural gas engines.
2. As engine speed increases, the excess air ratio also increases, resulting in a more obvious impact of fuel reforming on in-cylinder combustion performance.
3. Combustion with 12% fuel-reforming gases could enhance the indicated engine efficiency by 2% under a full-load condition of 1700 rpm but could have an adverse impact on the engine's power performance.
4. The emissions of NO_x and HC can be decreased significantly by increasing the fuel-reforming ratio. CH₄ emissions were reduced by up to 33%, and NO_x emissions were lowered by up to 20% at the full-load condition of 1200 rpm.

In general, a higher fuel-reforming ratio can improve emissions and economic performance for natural gas engines. However, increasing the reforming ratio requires more reforming of the fuel and air, which in turn requires more energy to heat the reforming gases. This poses a significant challenge in making the fuel reforming system practical for widespread use.

Author Contributions: Investigation, M.G.; Resources, J.Z.; Data curation, R.Z.; Writing—original draft, M.W.; Writing—review & editing, F.Y. All authors have read and agreed to the published version of the manuscript.

Funding: This research received no external funding.

Data Availability Statement: Data are contained within the article.

Conflicts of Interest: Authors Rui Zhou and Jian Zheng have received research grants from Shanghai Motor Vehicle Inspection Certification & Tech Innovation Center Co., Ltd.

Abbreviations

Φ	Equivalence ratio
BSFC	Brake-specific fuel consumption
°CA	Degrees crank angle
CA02	Crank angle of 2% mass fraction burnt
CA50	Crank angle of 50% mass fraction burnt
CO	Carbon monoxide
CO ₂	Carbon dioxide
CNG	Compressed natural gas
D-EGR	Dedicated EGR
HC	Hydrocarbon
NO _x	Nitrogen oxides
POFR	Partial oxidation fuel reforming
Rpm	Revolution per minute
SMR	Steam methane reforming
THC	Total hydrocarbon
WGS	Water-gas shift

References

1. Bae, C.; Kim, J. Alternative fuels for internal combustion engines. *Proc. Combust. Inst.* **2017**, *36*, 3389–3413. [[CrossRef](#)]
2. Khan, M.I.; Yasmin, T.; Shakoor, A. Technical overview of compressed natural gas (CNG) as a transportation fuel. *Renew. Sustain. Energy Rev.* **2015**, *51*, 785–797. [[CrossRef](#)]
3. Alois, K.; Heinz, H.; David, R.; Laura, L.; Robert, E.; Jean-François, L.; Kenneth, D.R.; Simon, G.; Heather, H.; Robin, N.; et al. *JEC Well-to-Wheels Report Version 4a*; Publications Office of the European Union: Luxembourg, 2014. [[CrossRef](#)]
4. Poulton, M.L. *Alternative Fuels for Road Vehicles*; Computational Mechanics Publications: London, UK, 1994.
5. Singh, S.; Mathai, R.; Singh, V.; Sehgal, A.K.; Basu, B.; Malhotra, R.K.; Nagarajan, S.; Yoganandam, S.; Kumar, G.S.; Gopal, G. *Effect of Hydrogen on the Performance & Emission Characteristics of a 6.0 L Heavy Duty Natural Gas Engine*; SAE Technical Paper 2014-01-2431; SAE: Warrendale, PA, USA, 2014. [[CrossRef](#)]
6. Alrazen, H.A.; Ahmad, K.A. HCNG fueled spark-ignition (SI) engine with its effects on performance and emissions. *Renew. Sustain. Energy Rev.* **2018**, *82*, 324–342. [[CrossRef](#)]
7. Lather, R.S.; Das, L.M. Performance and emission assessment of a multi-cylinder S.I engine using CNG & HCNG as fuels. *Int. J. Hydrogen Energy* **2019**, *44*, 21181–21192.
8. Michikawauchi, R.; Tanno, S.; Ito, Y.; Kanda, M.; Kawauchi, M. *Combustion Improvement of CNG Engines by Hydrogen Addition*; SAE Technical Paper, 2011-01-1996; SAE: Warrendale, PA, USA, 2011. [[CrossRef](#)]
9. Kim, J.; Chun, K.M.; Song, S.; Baek, H.K.; Lee, S.W. *Effect of Hydrogen as an Additive on Lean Limit and Emissions of a Turbo Gasoline Direct Injection Engine*; SAE Technical Papers; SAE: Warrendale, PA, USA, 2015. [[CrossRef](#)]
10. Alger, T.; Mangold, B. Dedicated EGR: A New Concept in High Efficiency Engines. *SAE Int. J. Engines* **2009**, *2*, 620–631. [[CrossRef](#)]
11. Robertson, D.; Chadwell, C.; Alger, T.; Zuehl, J.; Gukelberger, R.; Denton, B.; Smith, I. Dedicated EGR Vehicle Demonstration. *SAE Int. J. Engines* **2017**, *10*, 898–907. [[CrossRef](#)]
12. Mitchell, R.; Kocsis, M. *Performance Evaluation of Dedicated EGR on a 12 L Natural Gas Engine*; SAE Technical Paper, 2019-01-114; SAE: Warrendale, PA, USA, 2019. [[CrossRef](#)]
13. Thawko, A.; Persy, S.; Eyal, A.; Tartakovsky, L. *Effects of Fuel Injection Method on Energy Efficiency and Combustion Characteristics of SI Engine Fed with a Hydrogen-Rich Reformate*; SAE Technical Paper 2020-01-2082; SAE: Warrendale, PA, USA, 2020. [[CrossRef](#)]
14. Weiss, B.; Beutel, T.W.; Chapman, B.R.; Saathoff, J.D.; Merchant, S.; Majano, G.J.; Weissman, W. Onboard Natural Gas Reforming for Heavy Duty Vehicles. *SAE Int. J. Commer. Veh.* **2019**, *12*, 45–56. [[CrossRef](#)]
15. Gukelberger, R.; Gingrich, J.; Alger, T.; Almaraz, S. Potential and Challenges for a Water-Gas-Shift Catalyst as a Combustion Promoter on a D-EGR[®] Engine. *SAE Int. J. Engines* **2015**, *8*, 583–595. [[CrossRef](#)]
16. Yap, D.; Peucheret, S.M.; Megaritis, A.; Wyszynski, M.L.; Xu, H. Natural gas HCCI engine operation with exhaust gas fuel reforming. *Int. J. Hydrogen Energy* **2006**, *31*, 587–595. [[CrossRef](#)]
17. Long, Y.; Li, G.; Zhang, Z.; Liang, J. Application of reformed exhaust gas recirculation on marine LNG engines for NO_x emission control. *Fuel* **2021**, *291*, 120114. [[CrossRef](#)]
18. Zheng, J.; Zhou, R.; Zhan, R.; Lin, H. Combustion and emission characteristics of natural gas engine with partial-catalytic oxidation of the fuel. *Fuel* **2022**, *312*, 122796. [[CrossRef](#)]
19. Verlato, E.; Barison, S.; Cimino, S.; Dergal, F.; Lisi, L.; Mancino, G.; Musiani, M.; Vázquez-Gómez, L. Catalytic partial oxidation of methane over nanosized Rh supported on FeCrAlloy foams. *Int. J. Hydrogen Energy* **2014**, *39*, 11473–11485. [[CrossRef](#)]
20. Zheng, J.; Zhou, R.; Zheng, Z.; Zhang, Y.; Lin, H. Effects of excess air ratio and spark timing on performance and gaseous pollutant emissions of fuel reforming natural gas engine. *Int. J. Engine Res.* **2023**, *24*, 2649–2659. [[CrossRef](#)]
21. Dziubak, T.; Karczewski, M. Experimental Study of the Effect of Air Filter Pressure Drop on Internal Combustion Engine Performance. *Energies* **2022**, *15*, 3285. [[CrossRef](#)]
22. Varghese, R.J.; Kolekar, H.; Kumar, S. Laminar burning velocities of H₂/CO/CH₄/CO₂/N₂-air mixtures at elevated temperatures. *Int. J. Hydrogen Energy* **2019**, *44*, 12188–12199. [[CrossRef](#)]
23. Heywood, J.B. *Internal Combustion Engine Fundamentals*; McGraw-Hill: New York, NY, USA, 1988; pp. 567–659.
24. Liao, S.Y.; Jiang, D.M.; Cheng, Q. Determination of laminar burning velocities for natural gas. *Fuel* **2004**, *83*, 1247–1250. [[CrossRef](#)]
25. Kahraman, N.; Çeper, B.; Akansu, S.O.; Aydin, K. Investigation of combustion characteristics and emissions in a spark-ignition engine fuelled with natural gas–hydrogen blends. *Int. J. Hydrogen Energy* **2009**, *34*, 1026–1034. [[CrossRef](#)]

Disclaimer/Publisher’s Note: The statements, opinions and data contained in all publications are solely those of the individual author(s) and contributor(s) and not of MDPI and/or the editor(s). MDPI and/or the editor(s) disclaim responsibility for any injury to people or property resulting from any ideas, methods, instructions or products referred to in the content.